Available online at www.sciencedirect.com
ScienceDirect
Materials Science and Engineering C 28 (2008) 1242–1249
MATERIALS SCIENCE & ENGINEERING C
www.elsevier.com/locate/msec

Surface modification of poly(L-lactide) electrospun fibers with nanocrystal hydroxyapatite for engineered scaffold applications

Nguyen Dang Luong [a], Ik-Sang Moon [b], Doo Sung Lee [a], Young-Kwan Lee [c], Jae-Do Nam [a,*]

[a] Department of Polymer Science and Engineering, Sungkyunkwan University, Suwon, South Korea
[b] Department of Periodontology, Yongdong Severance Hospital, College of Dentistry, Yonsei University
[c] Department of Chemical Engineering, Sungkyunkwan University, Suwon, South Korea

Received 29 June 2006; accepted 14 November 2007
Available online 22 November 2007

Abstract

The hydrophobicity of the poly(L-lactide) (PLLA) surface was modified by incorporating hydroxyapatite (HAp) nanocrystalline particles during the electrospinning process for the engineered scaffold applications. The HAp nanocrystals were synthesized with 30 nm in diameter and 100–120 nm in length, which subsequently formed micrometer-sized agglomerates in the range of 2.5 μm. The synthesized HAp agglomerates were electrospun in the PLLA solution, and the HAp nanocrystals were desirably exposed on the surface of the electrospun PLLA fibers to give higher surface energy and lower contact angles with water. The surface-exposed hydrophilic HAp nanocrystals substantially increased the precipitation of various salts on the HAp/PLLA fiber surfaces in a buffer solution due to the hydrophilic nature and ionic affinity of HAp. Finally, the developed HAp/PLLA fibers desirably sustained the fibrous structural integrity during the accelerated-aging test in water, which was not the case with the pristine PLLA fibers.

Keywords: Electrospinning; Hydroxyapatite; Nanocomposite; PLLA; Surface modification

1. Introduction

Biodegradability and ability to induce and promote the new bone formation by osteogenic cells at grafted sites are the prerequisites of graft materials in the field of the bone regeneration like implant dentistry and periodontology [1]. The critical properties of bone-graft materials to be used in the load-bearing sites are the degree of strength retention over time, and the structural and mechanical equivalence to the bone with the proper biodegradation rates [2]. Engineered scaffold structures usually in the form of porous structures need to provide a mechanical modulus ranging from 10 to 1,500 MPa for hard tissue and 0.4 to 350 MPa for soft tissue applications [3], which correspond to the mechanical properties of human tissues [4]. Polymeric porous scaffold structures have been fabricated using traditional polymer-processing techniques such as porogen leaching or gas forming [5]. However, the maximum compressive moduli of those processes and material systems are in the range of ca. 0.4 MPa, which is well below the requirements for hard tissue or most soft tissue applications [6]. Recently, a nanocomposite technology has been adopted to reinforce the polymer scaffold structure, for example, by using nano-sized reinforcing entities like montmorillonite (MMT) [7]. When a small amount of MMT platelets (5.79 vol. %) is added to PLLA polymers, the tensile modulus of the MMT/PLLA composite system was reported to increase up to 170.1 MPa [7a].

HAp represents a family of bone grafting materials which have been focused on in the last decades because it contains biocompatibility with little inflammatory response when implanted within connective and bone tissues [8]. In addition, as with the MMT/PLLA scaffold systems [7], the HAp particles can act as reinforcing entities when incorporated in biodegradable polymers, which can ultimately give a mechanically-robust engineered scaffolds. Excellent biocompatibility and promising bioactivity of HAp stem from the similar compositions to the bone and tooth minerals [9]. A polymer-based HAp implant system prepared by an image-based design with orthogonal channels (40% porosity) was reported to provide a compressive modulus and strength of 1400±400 MPa and 30±8 MPa, respectively

* Corresponding author. Tel.: +82 31 290 7285; fax: +82 31 292 8790.
E-mail address: jdnam@skku.edu (J.-D. Nam).

0928-4931/$ - see front matter © 2007 Elsevier B.V. All rights reserved.
doi:10.1016/j.msec.2007.11.005

[10]. When the HAp-polyacrylamide composite scaffold was fabricated by combining the gel casting and polymer sponge techniques, a compressive strength of 9.8±0.3 MPa was reported, which was comparable to the high-end value (2–10 MPa) of cancellous bone [11].

In addition to the enhancement of mechanical properties, the bone bonding and osteoconductive capacity of HAp have demonstrated it to be a good biocompatible implant material [12]. HAp has excellent biocompatibility, bioactivity, osteoconduction characteristics [13], and surface activity with living tissue [14] and, further, they allow osteogenesis to occur to form tight bonds with host tissue [11]. It should also be addressed that the nano-sized HAp particles can provide an extremely large surface area and high surface energy, which may provide substantially different mechanical properties and bioactivity of HAp nanocomposite systems. Subsequently, we synthesized the HAp nanocrystals in this study using a liquid-phase chemical precipitation method to control the HAp particulate sizes down to the nanometer scale with a narrow size distribution [15].

The electrospinning process offers unique capabilities for producing novel synthetic fibers with an unusually small diameter and good mechanical performance [16]. In particular, this process is considered to be an attractive approach for fabricating fibrous biomaterials for applications such as tissue engineering, vascular grafts, tissue repair, wound healing, and drug delivery [17,18]. For example, an electrospun scaffold structure has been fabricated to produce a scaffold system containing dual-sized porosity distribution by combining the electrospinning and salt-leaching techniques [18]. The electrospun fibrous structure can provide a facile transport of metabolic nutrients and waste through the nanometer-sized pores, and the efficient cell implantation and blood vessel invasion can be expected through the micrometer-sized pores [18]. Although the structural morphology of electrospun polymer fibers is desirable in scaffold applications, the surface property of most polymeric materials is hydrophobic in nature and, thus, it is not favorable to human cellular adhesion. In this sense, it is needed to modify the hydrophobic surface of electrospun polymer fibers, for example, incorporating the hydrophilic and bioactive HAp nanoparticles in biodegradable polymers especially on the exposed surfaces. It should also be addressed that the incorporated HAp nanoparticles can also act as a reinforcement to give an increased mechanical strength and structural integrity during the bone regeneration processes.

In this study, HAp was synthesized by a chemical precipitation method and incorporated into the PLLA solution. The surface energy and structural integrity of the electrospun HAp/PLLA composite fibers were investigated to give desirable surface characteristics and improved biodegradation behaviors for hard-tissue scaffold applications.

2. Materials and methods

2.1. Materials

The $Ca(NO_3)_2 \cdot 4H_2O$ (99%), $(NH_4)_2HPO_4$ (99%), ammonium hydroxide solution, poly(L-lactide) (M_W 85,000–160,000), polyvinylpyrrolidone(PVP)(M_W 40,000) and chloroform were purchased from the Sigma–Aldrich Corporation. Deionized (DI) water was used throughout all experiments. All other reagents were of commercially available analytical grade and used as received.

2.2. Synthesis of hydroxyapatite

Nanocrystalline HAp was synthesized using a chemical precipitation method [11]. Each of $Ca(NO_3)_2 \cdot 4H_2O$ and $(NH_4)_2HPO_4$ was dissolved in deionized water to form 0.5 M aqueous solutions. Then, PVP was dissolved in the $Ca(NO_3)_2 \cdot 4H_2O$ solution at 7 weight percent (wt.%), 15 wt.%, 25 wt.% and 100 wt.% with respect to the solid content of $Ca(NO_3)_2 \cdot 4H_2O$. Subsequently equal amounts of $Ca(NO_3)_2 \cdot 4H_2O$ and $(NH_4)_2HPO_4$ aqueous solutions were mixed under constant magnetic stirring at room temperature. Ammonium hydroxide was added immediately in order to maintain at the pH at 10, which was kept constant throughout the experiment. After ripening at ambient temperature for 72 h, the precipitates were recovered by centrifugation and washed with DI water to remove PVP. Five cycles of washing and centrifugation were repeated in order to ensure the complete removal of byproducts. The synthesized powders were calcinated at 800 °C for 1 h in nitrogen.

2.3. Electrospinning

The electrospinning set-up consisted of a syringe needle and a DC high voltage power supply. A positive voltage was applied to the polymer solution using a power supply (HYP-303D, Han Young Co., Korea) at 3–10 kV. A HAp/PLLA mixture was prepared by mixing the HAp powder in a chloroform solution of poly(L-lactide) (1:10 w/w of HAp to PLLA) with two different mixing conditions: (i) at room temperature for 48 h and (ii) at 70 °C for 5 h, each corresponding to a poor and good mixing condition of particle dispersion, respectively. The HAp/PLLA mixture was electrospun at a constant mass flow rate of 1 ml/h [19].

2.4. Biodegradation experiments

For the biodegradation experiments, the electrospun PLLA and HAp/PLLA fibers were hydrolyzed in water at 60 °C and in a buffer solution at 38 °C. The buffer solution was composed of 135 mM of NaCl, 5 mM of KCl, 1 mM of $MgCl_2$, 10 mM of *N*-(2-hydroxyethyl)-piperazine-*N*'-2-ethanesulfonic acid $C_8H_{18}N_2O_4S$ (HEPES), 1 mM of $CaCl_2$, and 10 mM of glucose, which were adjusted at pH 7.4 using a 1 N NaOH solution.

2.5. Measurements

The phase composition and crystallinity of the "as-dried" and "calcinated" HAp were analysed by wide angle X-ray diffraction (Mac Science, Mac-18xhf). CuKα radiation ($\lambda = 0.154$ nm) and a curved graphite crystal monochromator was used in the measurements. The applied voltage and current of the X-ray tubes were 30 kV and 100 mA, respectively. The data was collected in the 2θ range between 20 and 60° with a scanning

speed of 5°/min. The aggregated particle size of the HAp powder was further analyzed by a particle size analyzer (Zetasizer 1000HS). The morphology of the HAp and the electrospun fibers was analyzed by a scanning electron microscopy (Hitachi S-2140). For the Infrared (IR) analysis (MATTSON 5000), the PLLA and HAp/PLLA electrospun fiber samples were dissolved in chloroform for 1 day and cast as a transparent thin film. The water contact angle and surface energy of HAp/PLLA systems were measured by a contact angle meter (GBX DIGIDROP-Scientific Instrumentation) using the same thin-film specimens as prepared for the IR analysis.

3. Results and discussion

3.1. Synthesis of hydroxyapatite

Fig. 1 shows the SEM images and XRD patterns of HAp powders comparing before and after calcinations (100 wt.% of PVP concentrations with respect to the solid content of $Ca(NO_3)_2 \cdot 4H_2O$ at pH = 10). In the SEM image before calcinations (Fig. 1A), the shape of the HAp is not well developed exhibiting obscure particulate boundaries. In the SEM image after calcination (Fig. 1B), however, the boundaries of HAp crystalline particles can be seen as a rod shape at approximately 30 nm in diameter and 100–120 nm in length. The size of the synthesized HAp nanorods may be compared well with the HAp particles existing in the human body: 130 × 30 nm in teeth enamel and 20 × 4 nm in dentine and bones [20,21]. These primary crystallites in the nanometer scale aggregated by the interparticle bonding to form agglomerates [21] in ca. 2.5 μm of diameters (see the result of particle size analysis in the Supporting information). The XRD results of HAp powders in the Fig. 1 compare the as-dried (Fig. 1A) and calcined powders (Fig. 1B). The XRD spectra of both systems exhibit the HAp characteristic peaks [11,22]. In particular, the peak at 31.8° (the strongest intensity peak) corresponds to the hydroxyapatite (211) diffraction peak, which is a strong evidence of HAp and a strong evidence for the crystallinity of HAp. Comparing the specimens before and after calcination, the as-dried HAp powders appear poorly crystalline, but the crystallinity of the calcinated HAp powder increases markedly after calcination at 800 °C. For example, the lattice planes of HAp at (200), (111), (300), (301), (131), etc. can be clearly seen in calcined sample, which is not the

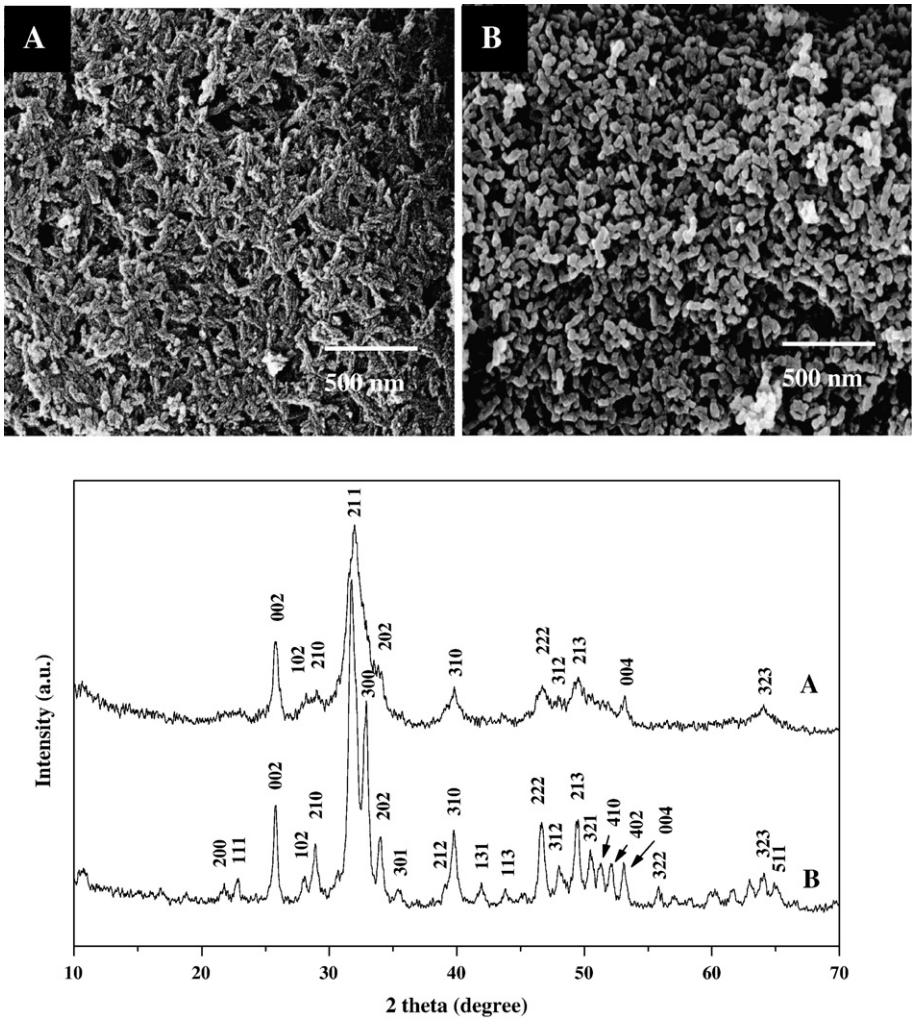

Fig. 1. SEM micrographs of the synthesized HAp nanocrystals in the state of as-dried powders (A) and calcined powders (B) synthesized at 100 wt.% of PVP stabilizer, and XRD of HAp nanocrystals for (A) as-dried powder and (B) calcined powder.

case with as-dried sample. Upon calcination at 800 °C, the level of crystallinity is believed to increase dramatically as revealed by the sharpened and distinct peaks in the 2θ angle range of 30–35°. The splitting of the broadened peaks in the 2θ angle region of approximately 31–34° for the powder after calcination indicate that it possesses a higher level of crystallinity and a larger average crystallite size than as-dried powders.

3.2. Fabrication of HAp/PLLA composite fiber using electrospinning

Fig. 2 shows SEM images of the electrospun fibers of the various HAp/PLLA systems. The pristine PLLA fibers show a smooth and uniform fiber surface with 1–3 μm of diameter (Fig. 2A and B). Fig. 2C and D show that the HAp/PLLA composite fibers containing 10 wt.% HAp mixed at room temperature, which correspond to a relatively poor dispersion condition of HAp, have an irregular and undulating surface morphology with substantial variations in diameter along the fiber direction. In this case, the electrospun fiber diameters range from 2 to 6 μm and the HAp particles appear to agglomerate in the mixture to form undulated fiber surfaces. Fig. 2E and F show the HAp/PLLA fibers containing 10 wt.% HAp mixed at 70 °C, which represents a good mixing condition. When mixing is performed at high temperature (70 °C) for 5 h, the fiber diameters appear fairly uniform with 5–10 μm, which is slightly larger than the ones electrospun in the bad mixing condition. It can be also seen that a larger number of HAp particles are exposed on the surface of the PLLA composite fibers. It is believed that a good dispersion of the HAp particles in the PLLA solution results in a uniform fiber diameter and good HAp exposure on the electrospun fiber surfaces. We believe that the mixing condition of HAp in the polymer solution substantially influences the final morphology of the electrospun fibers. The surface-exposed HAp particles may well enhance the hydrophilicity and biocompatibility of scaffold systems.

Fig. 3 compares the IR spectra of the pristine PLLA (Fig. 3A) and HAp/PLLA composite (10 wt.% of HAp) (Fig. 3B) fibers for the HAp mixing condition at 70 °C for 5 h. The C=O absorbance peak at 1760 cm^{-1} in the poly(L-lactide) chains has been used as a typical PLLA characteristic peak, which can be observed in both Fig. 3A and B [23,24]. For the HAp/PLLA composite fibers shown in Fig. 3B, the characteristic peaks of HAp, corresponding to the stretching vibration of PO_4^{3-}(956; 1047; 1099 cm^{-1}) and deformation vibrations of PO_4^{3-}(563; 605 cm^{-1}) can be identified, which do not appeared in the case of PLLA fibers. The weak absorption peak at 871 cm^{-1} (P–O–H vibration in the HPO_4^{2-}), can also be confirmed [15 a,23,25,26]. The results demonstrate that the HAp particles are successfully incorporated into the electrospun HAp/PLLA fibers.

3.3. Contact angle and surface free energy

The surface energy characteristics of engineered scaffolds substantially influence interactive processes taking place at the interphase between the human tissue and the implant surface [27]. It is the surface of a scaffold that first comes into contact with a living body; hence, the initial response of cells to the biomaterial mostly depends on the surface properties of scaffolds [28]. Cellular

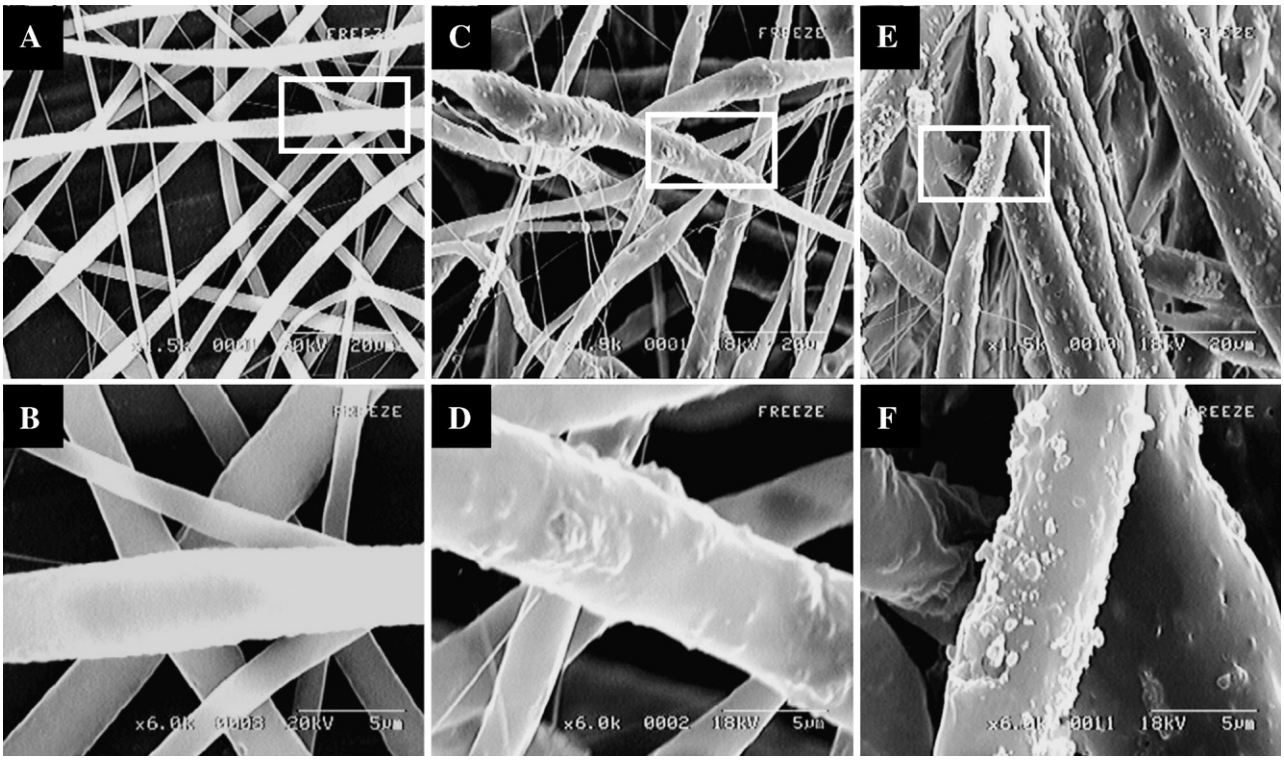

Fig. 2. SEM micrographs of the electrospun fibers of the pristine PLLA (A, B), HAp/PLLA mixed at room temperature for 48 h (C, D), and HAp/PLLA mixed at 70 °C for 5 h (E, F). The HAp content with respect to PLLA was fixed at 10 wt.%.

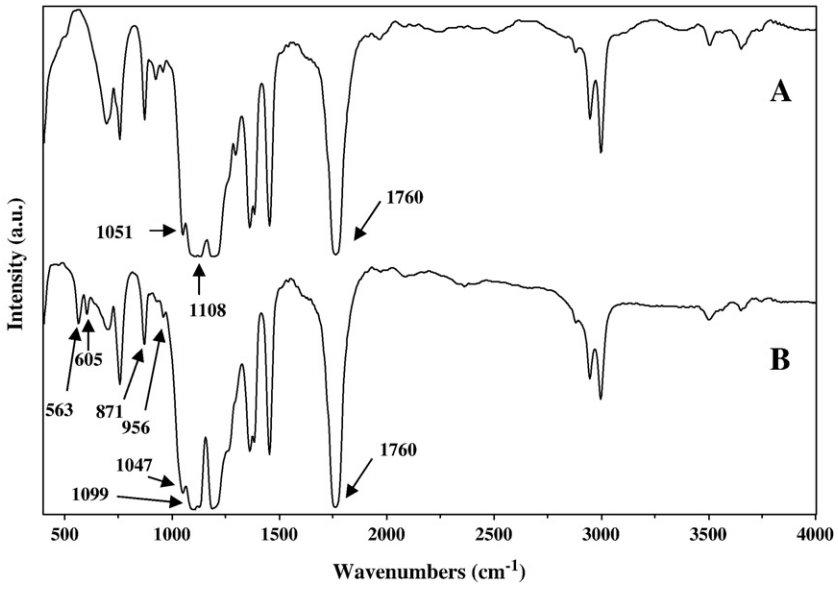

Fig. 3. IR spectra of the electrospun fibers comparing (A) pristine PLLA fiber and (B) HAp/PLLA composite fiber (10 wt.% HAp). HAp particles were mixed with PLLA solution at 70 °C for 5 h.

adhesion is affected by the hydrophilic property, structure, and chemical composition of the scaffold surface [28–32]. These factors also influence cellular proliferation, migration, and physiological response [29]. Appropriate modification of the surface characteristics of the scaffold increases cell adhesion, proliferation, migration, and differentiation [28–32]. One of the simplest methods of estimating the surface adhesion properties of materials may be the contact angle [32]. Generally, determination of solid surface tensions from contact angles starts with the Young equation [33], which describes the energy balance of a liquid drop on a solid surface. This equation can be expressed as

$$\gamma_l \cos\theta = \gamma_s - \gamma_{sl} \quad (1)$$

where θ is the contact angle (degree), γ_l, γ_s, and γ_{sl} are the surface free energy of the liquid, the surface free energy of the solid, and the interfacial free energy between the liquid and the solid (mJ m^{-2}), respectively. The pristine PLLA polymer film shows a water contact angle at 76.3° with the surface energy values of γ_s=29.52 mJ m^{-2}, γ_s^d=15.81 mJ m^{-2}, and γ_s^p=13.71 mJ m^{-2}, and the HAp/PLLA system, which contains 10 wt.% of HAp mixed at 70 °C for 5 h, shows 67.7° with surface energy values of γ_s=34.66 mJ m^{-2}, γ_s^d=9.44 mJ m^{-2}, and γ_s^p =25.22 mJ m^{-2}. The γ_s^d and γ_s^p are the dispersion and polar components of the surface free energy [33], respectively, which were determined by comparing the contact angles of water and ethylene glycol in this study [34]. It demonstrates that the nanocrystalline HAp particles make the PLLA fiber surface more hydrophilic by increasing the surface energy, especially increasing the polar component of the surface energy. It is believed that the increased hydrophilicity of the HAp/PLLA composite system can enhance the biocompatibility of the scaffold surface with respect to human cells.

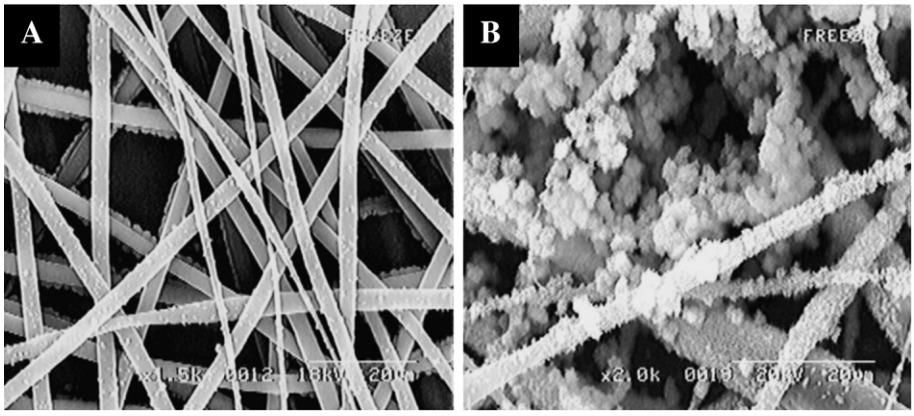

Fig. 4. SEM micrographs of (A) pristine PLLA fiber and (B) HAp/PLLA composite fiber after biodegradation in buffer solution at 38 °C for 48 h. The HAp/PLLA fiber contains 10 wt.% of HAp mixed with PLLA solution at 70 °C for 5 h.

3.4. Biodegradation experiments

The SEM micrographs in Fig. 4 show the surface morphologies of the pristine PLLA (Fig. 4A) and HAp/PLLA composite fibers (Fig. 4B) after immerging them in the buffer solution at 38 °C for 48 h. As shown in Fig. 4B, the ions included in the buffer solution precipitate to form non-soluble salt particles (most probably calcium-based salts) on the surface of the HAp/PLLA composite fibers to a large extent, which is not the case with the pristine PLLA fibers (Fig. 4A). The facile precipitation process of ions in buffer solution on HAp/PLLA composite fiber surfaces may be assumed to occur due to the ionic affinity of HAp with the ions in buffer solution. The absorption of solutes from the aqueous solutions to the HAp/PLLA surface may take place by the formation of a surface complex or the chemical reaction with calcium or phosphate ions of HAp to form the precipitates out of the solution [35]. The surface-exposed HAp particles on the PLLA fibers improve the hydrophilicity of the pristine PLLA, which may very well improve the *in vivo* cytocompatibility of PLLA composite fibers [28]. Due to the hydrophilic nature and ionic affinity of nanocrystalline HAp particles, there is a strong possibility that the osteogenic cells can be effectively grafted at the HAp sites to be promoted because it has been widely accepted that human cells prefer to attach to hydrophilic surfaces than hydrophobic surfaces [31].

Furthermore, the biodegradation behavior of the PLLA/HAp systems was investigated in an accelerated condition at 60 °C of DI water. Fig. 5 compares the pristine PLLA fibers (Fig. 5A, B, and C) and HAp/PLLA composite fibers (Fig. 5D, E and F, which were synthesized with a mixing condition at 70 °C for 5 h) aged for 24, 72 and 96 h, respectively. After the pristine PLLA fibers are aged for 72 h (Fig. 5B), the fiber surface starts being fragmented. After 96 h of aging, it can be seen that the PLLA fiber is completely fragmented (Fig. 5C). However, when HAp particles are included in the PLLA fibers, the fibrous structure is clearly sustained after 24, 72 and 96 h of aging (Fig. 5D, E and F). This clearly demonstrates that the HAp nano-sized entities effectively slow the biodegradation process of the PLLA electrospun fibers.

The biodegradation of PLLA in water take places when the ester groups in the PLLA macromolecules are hydrolyzed [36]. In the HAp/PLLA composite fibers, the ester groups (COO^-) in PLLA molecules are bound with Ca^{2+} ions of HAp by the ionic interaction, and thus the hydrolysis reaction of the ester groups in PLLA may be suppressed by the ionic bonding [35a]. In most polymeric composite systems, the filler–matrix interactions have a great effect on increasing the chemical resistance and the thermo-oxidative stability by the presence of additive entities [37]. The similar composite effect is expected to occur in the composite system to give an enhanced resistance to the hydrolysis reaction. It is also believed that this interphase-bonding effect of the filler can be increased when the particle size is further reduced because the interphase area is substantially increased in the composite system. Conclusively, the interphase layer is formed between the PLLA molecules and HAp particles in our composite system due to the ionic interaction between the COO^- groups in PLLA and Ca^{2+} ions in

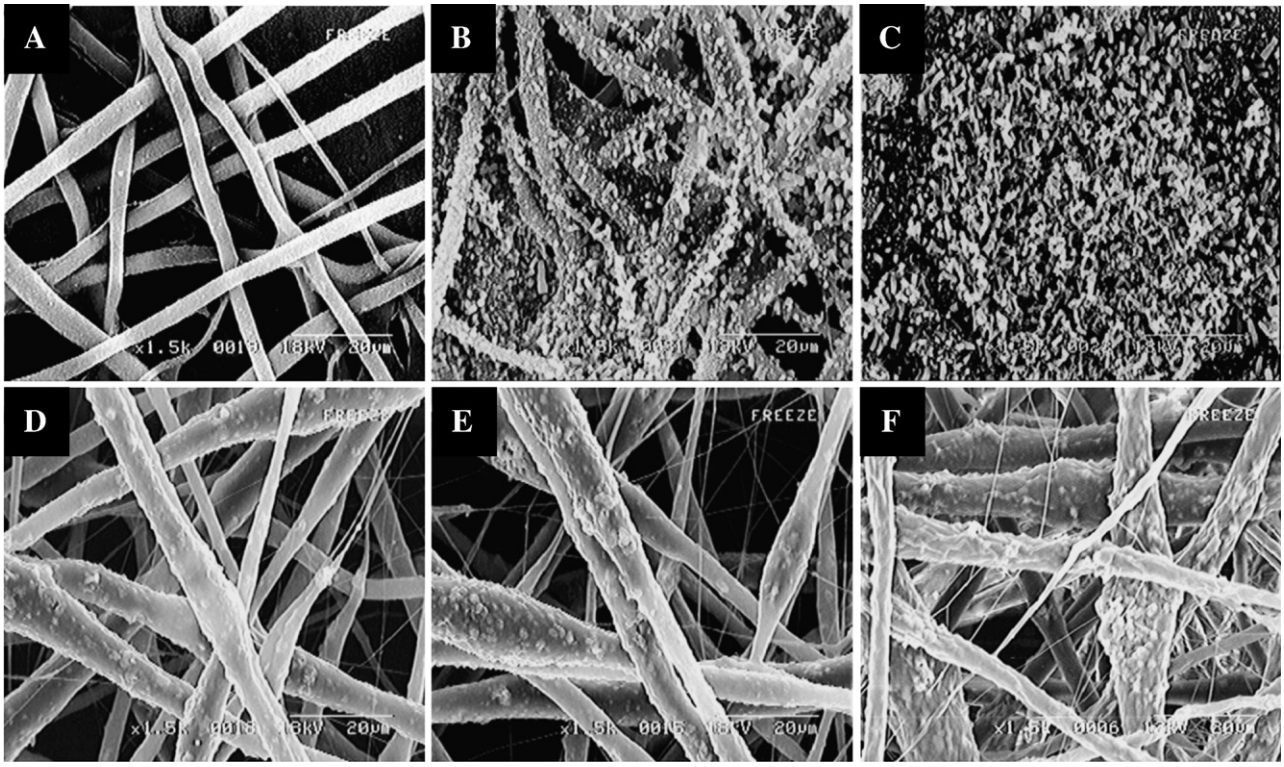

Fig. 5. SEM micrographs of the PLLA fiber (A, B, C) and HAp/PLLA composite (D, E, F) after biodegradation in DI water at 60 °C for 24, 72 and 96 h, respectively. The HAp/PLLA fiber contains 10 wt.% of HAp mixed with PLLA solution at 70 °C for 5 h.

HAp to suppress the hydrolysis reaction and enhance the structural stability during biodegradation reaction.

We believe that the sustainability of the HAp incorporation could desirably enhance the guided bone regeneration process by securing the scaffold skeletal structure and the pore space during biodegradation, which is highly required for the bone regeneration. The developed technique demonstrates a great potential to tailor the surface cytocompatibilization and *in vivo* biodegradation characteristics of the engineered scaffolds further through the optimization of the HAp-particle morphology, biodegradable polymers, and their composite formation process.

4. Conclusions

The HAp nanocrystals were synthesized and incorporated into PLLA polymer solutions. The mixing (or dispersion) conditions of HAp particles influenced the resulting morphology of electrospun fibers of HAp/PLLA composite systems. The electrospun HAp/PLLA composite fibers exhibited an improved hydrophilicity and bioactivity due to the surface-exposed HAp particles, and the structural sustainability of the composite system was demonstrated by the accelerated biodegradation experiments.

4.1. Supporting information available

Details of description and Supplement figures about SEM, XRD, IR, and particle size analysis of the synthesized HAps.

Acknowledgement

This work was supported by the Korea Research Foundation Grant (KRF-2004-005-D00063). We also appreciate project and equipment support from Gyeonggi Province and SAINT through Gyeonggi Regional Research Center at Sungkyunkwan University.

Appendix A. Supplementary data

Supplementary data associated with this article can be found, in the online version, at doi:10.1016/j.msec.2007.11.005.

References

[1] F. Zhao, Y. Yin, W.W. Lu, J.C. Leong, W. Zhang, F. Zhang, M. Zhang, K. Yao, Biomaterials 23 (2002) 3227.
[2] E. Ural, K. Kesenci, L. Fambri, C. Migliaresi, E. Piskin, Biomaterials 21 (2000) 2147.
[3] R.W. Goulet, S.A. Goldstein, M.J. Ciarelli, J.L. Kuhn, M.B. Brown, L.A. Feldkamp, J. Biomech. 27 (1994) 375.
[4] [a] K. Hayashi, Biomechanics of soft tissue in cardiovascular systems, Springer, New York, 2003;
[b] K.A. Hing, S.M. Best, W. Bonefield, J. Mater. Sci., Mater. Med. 10 (1999) 135;
[c] J.F. De Oliverira, P.F. De Aguiar, A.M. Rossi, G.A. Soares, Int. Soc. Art. Org. 27 (2003) 406.
[5] [a] P.X. Ma, J.W. Choi, Tissue Eng. 7 (2001) 23;
[b] W.L. Murphy, R.G. Dennis, J.L. Kileny, D.J. Mooney, Tissue Eng. 8 (2002) 43.
[6] S.J. Holloster, Nat. materials 4 (2005) 518.
[7] [a] J.H. Lee, T.G. Park, H.S. Park, D.S. Lee, Y.K. Lee, S.C. Yoon, J.D. Nam, Biomaterials 24 (2003) 2773;
[b] J.H. Lee, Y.H. Lee, D.S. Lee, Y.K. Lee, J.D. Nam, Polymer (Korea) 29 (2005) 375.
[8] A. Scabbia, L. Trombelli, J. Clin. Periodontol. 31 (2004) 348.
[9] [a] R.H. Doremus, J. Mater. Sci. 27 (1992) 285;
[b] E.B. Nery, K.L. Lynch, W.M. Hirthe, K.H. Mueller, J. Periodontol. 46 (1975) 328;
[c] R. LeGeros, J. LeGeros, in: J.O. Nriagu, P.B. Moore (Eds.), Phosphate Minerals, Springer, Berlin, 1984, p. 351;
[d] L.L. Hench, J. Am. Ceram. Soc. 74 (1991) 1487.
[10] T.M. Chu, D.G. Orton, S.J. Hollister, S.E. Feinberg, J.W. Halloran, Biomaterials 23 (2002) 1283.
[11] R.R. Hassna, M. Zhang, Biomaterials 25 (2004) 5171.
[12] [a] G.T. Cra, I.M. Brook, D.J. Lamb, Biomaterials 10 (1989) 133;
[b] M. Ito, Biomaterials 12 (1991) 41.
[13] S.H. Kwon, Y.K. Jun, S.H. Hong, H.E. Kim, J. Eur. Ceram. Soc. 23 (2003) 1039.
[14] K.C.B. Yeong, J. Wang, S.C. Ng, Biomaterials 22 (2001) 2705.
[15] [a] W. Kim, Q.W. Zhang, F. Saito, J. Mater. Sci. 35 (2000) 5401;
[b] A.C. Tas, J. Eur. Ceram. Soc. 20 (2000) 2389;
[c] M. Jarcho, C.H. Bolen, M.B. Thomas, J. Bobick, J.F. Kay, R.H. Doremus, J. Mater. Sci. 11 (1976) 2027;
[d] J.L. Xu, K.A. Khor, Y.W. Gu, R. Kumar, P. Cheang, Biomaterials 26 (2005) 2197;
[e] L.Y. Huang, K.W. Xu, J. Lu, J. Mater. Sci., Mater. Med. 11 (2000) 667;
[f] W.J. Weng, J.L. Baptista, Biomaterials 19 (1998) 125;
[g] W.J. Weng, J.L. Baptista, J. Mater. Sci., Mater. Med. 9 (1998) 159;
[h] H. Katsuki, S. Furuta, S. Komarneni, J. Am. Ceram. Soc. 82 (1999) 2257;
[i] M. Yoshmura, H. Suda, K. Okmoto, K. Loku, J. Mater. Sci. 29 (1994) 3399;
[j] G.K. Lim, J. Wang, S.C. Ng, L.M. Gan, Langmuir 15 (1999) 7472.
[16] [a] J.M. Deitzel, J. Kleinmeyer, D. Harris, N.C. Beck Tan, Polymer 42 (2001) 261;
[b] J. Zeng, X.S. Chen, X.Y. Xu, Q.H. Liang, X.C. Bian, L.X. Yang, X.B. Jing, J. App. Polym. Sci. 89 (2003) 1085.
[17] [a] S.P. Zhong, W.E. Teo, X. Zhu, R. Beuerman, S. Ramakrishna, L.Y.L. Yung, Biomacromolecules 6 (2005) 2998;
[b] E.D. Boland, G.E. Wnek, D.G. Simpson, K.J. Pawlowski, G.L. Bowlin, J. Macromol. Sci. 38 (2001) 1231;
[c] J.D. Stitzel, K. Pawlowski, G.E. Wnek, D.G. Simpson, G.L. Bowlin, J. Biomater. Appl. 15 (2001) 1;
[d] J.A. Matthews, G.E. Wnek, D.G. Simpson, G.L. Bowlin, Biomacromolecules 3 (2002) 232;
[e] I.K. Kwon, T. Matsuda, Biomacromolecules 6 (2005) 2096;
[f] E.R. Kenawy, G.L. Bowlin, K. Mansfield, J. Layman, E. Sanders, D.G. Simpson, G.E. Wnek, J. Control. Release 81 (2002) 57;
[g] W.J. Li, C.T. Laurencin, E.J. Caterson, R.S. Tuan, F.K. Ko, J. Biomed. Mater. Res. 60 (2002) 613;
[h] X. Zong, K. Kim, D. Fang, S. Ran, B. Hsiao, B. Chu, Polymer 43 (2002) 4403.
[18] Y.H. Lee, J.H. Lee, I.G. An, C. Kim, D.S. Lee, Y.K. Lee, J.D. Nam, Biomaterials 26 (2005) 3165.
[19] R.A.N. odrigues da Silva, R. Furlan, I. Ramos, J.J. Santiago-Aviles, Mater. Res. 8 (2005) 105.
[20] R.Z. LeGeros, Monographs in Oral Science, Karger, New York, 1991.
[21] [a] A.D. Randolph, M.A. Larson, Theory of Particulate Processes: Analysis and techniques of continuous crystallization, Academic Press, New York, 1986;
[b] R. Rodriguez-Clemente, A. Lopez-Macipe, J. Gomez-Morales, J. Torrent-Burgues, V.M. Castano, J. Eur. Ceram. Soc. 18 (1998) 1351.
[22] PDF Card No 9-432, ICDD, Newtown Square, Pennsylvania, USA.
[23] I.N. gnjatovic, V. Savic, S. Najman, M. Plavsic, D. Uskokovic, Biomaterials 22 (2002) 571.
[24] P.H. Nam, A. Fujimori, T. Masuko, e-Polymers 005, 2003, p. 1.
[25] [a] M.C. Chang, C.C. Ko, W.H. Douglas, Biomaterials 24 (2003) 3087;
[b] M. Chu, G. Liu, Nanotechnology 16 (2005) 1208;

[c] M.C. Pina, E. Villareal, S. Martin, B. Leon, G. Torres-Villasenor, P. Bosch, J. Appl. Biomater. Biomech. 2 (2004) 112.
[26] [a] X. Wanga, Y. Yubao Lia, J. Weia, K. de Grootb, Biomaterials 23 (2002) 4787;
[b] A. Sinha, S. Nayar, A. Agrawal, D. Bhattacharyya, P. Ramachandrarao, J. Am. Ceram. Soc. 86 (2003) 357.
[27] S. Hanson, B.D. Ratner, in: B.D. Ratner, A.S. Hoffman, F.J. Schoen, J.E. Lemons (Eds.), An Introduction to Materials in Medicine, Academic Press, New York, 1996, p. 228.
[28] [a] Y. Zhu, C. Gao, T. He, X. Liu, J. Shen, Biomacromolecules 4 (2003) 446;
[b] Z. Ma, C. Gao, Y. Gong, J. Ji, J. Shen, J. Biomed. Mater. Res. (Appl. Biomater.) 63 (2002) 838.
[29] R.K. Sinha, F. Morris, S.A. Shah, R.S. Tuan, Clin. Orthop. Relat. Res. 305 (1994) 258.
[30] Y.C. Wu, S.Y. Shaw, H.R. Lin, T.M. Lee, C.Y. Yang, Biomaterials 27 (2006) 896.
[31] Z. Ma, C. Gao, J. Yuan, J. Ji, J. Shen, J. Appl. Polym. Sci. 85 (2002) 2163.
[32] N. Dumitrascu, C. Borcia, J. Colloid Interface Sci. 294 (2006) 418.
[33] [a] M.E. Schrader, Langmuir 12 (1996) 3728;
[b] D.Y. Kwok, A. Leung, C.N.C. Lam, A. Li, R. Wu, A.W. Neumann, J. Colloid Interface Sci. 206 (1998) 44;
[c] M.O. Goebel, J. Bachmann, S.K. Woche, W.R. Fischer, R. Horton, Soil Sci. Soc. Am. J. 68 (2004) 383;
[d] B. Janczuk, T. Bialopiotrowicz, W. Wojcik, J. Colloid Interface Sci. 127 (1989) 59.
[34] Contact angles of ethylene glycol for the pristine PLLA and HAp/PLLA systems were 55.3 ° and 52.9°, respectively. These angles and the water contact angles were substituted into the following equation to calculate γ_s^d, γ_s^p and γ_s of PLLA and HAp/PLLA systems [[33c]] $1+\cos\theta = 2\sqrt{\gamma_s^d}\left(\frac{\sqrt{\gamma_l^d}}{\gamma_l}\right)+2\sqrt{\gamma_s^p}\left(\frac{\sqrt{\gamma_l^p}}{\gamma_l}\right)$, $\gamma_l=\gamma_l^d+\gamma_l^p$, and $\gamma_s=\gamma_s^d+\gamma_s^p$ where γ_l^d=29.29 mJ m^{-2}, γ_l^p=18.91 mJ m^{-2}, and γ_l=48.20 mJ m^{-2} for ethylene glycol, and γ_l^d=21.80 mJ m^{-2}, γ_l^p=51.00 mJ m^{-2}, and γ_l=72.80 mJ m^{-2} for water [[33d].
[35] [a] H. Maeda, T. Kasuga, M. Nogami, J. Am. Ceram. Soc. 88 (2005) 1964;
[b] D.N. Misra, J. Biomed. Mater. Res. (Appl. Biomater.) 48 (1999) 848.
[36] X.S. Wu, Encyclopedic handbook of biomaterials andbioengineering, Marcel Dekker, New York, 1995.
[37] [a] J. Manhart, K.H. Kunzelmann, H.Y. Chen, R. Hickel, Dent. Mat. 16 (2000) 33;
[b] F. Yang, G.L. Nelson, Polym. Adv. Technol. 17 (2006) 320.